crystals

MDPI

Article

The Effects of a Mixed Precipitant on the Morphology and Electrochemical Performance of $LiNi_{0.5}Mn_{1.5}O_4$ Cathode Materials

Yang Shu [1,2,†], Wenchao Yan [2,†], Haisong Wang [1,*], Jicheng Jiang [2], Deye Sun [2], Xiaodi Ma [2] and Yongcheng Jin [2,*]

1 School of Light Industry and Chemical Engineering, Dalian Polytechnic University, Dalian 116034, China; sy12255471@gmail.com

2 Qingdao Institute of Bioenergy and Bioprocess Technology, Chinese Academy of Sciences, Qingdao 266101, China; yanwc@qibebt.ac.cn (W.Y.); jiangjc@qibebt.ac.cn (J.J.); sundy@qibebt.ac.cn (D.S.); maxd@qibebt.ac.cn (X.M.)

* Correspondence: wanghaisong@163.com (H.W.); jinyc@qibebt.ac.cn (Y.J.); Tel.: +86-411-8632-3272 (H.W.); +86-532-8066-2703 (Y.J.)

† These authors contributed equally to this work.

Academic Editors: Lan Xiang, Jing Wang, Huijun Wu, Guo Gao, Yongcheng Jin and Yi Xia
Received: 2 August 2017; Accepted: 8 September 2017; Published: 14 September 2017

Abstract: A series of $LiNi_{0.5}Mn_{1.5}O_4$ (LNMO) samples were synthesized by adjusting the molar ratio of $(NH_4)_2CO_3$ to Na_2CO_3 in a mixed precipitant for evaluating the effects of ammonia from $(NH_4)_2CO_3$ as a complexing agent and Na_2CO_3 as a precipitant on the morphology and electrochemical performances of LNMO. In this research, a rapid precipitation method followed by hydrothermal treatment was used to prepare the precursors of LNMO, and different molar ratios (0:1, 1:2, 1:1, 2:1, 1:0) of $(NH_4)_2CO_3$ to Na_2CO_3 were used for mixed precipitants. The test results revealed that the cathode material exhibits the best electrochemical performance when the molar ratio of $(NH_4)_2CO_3$ to Na_2CO_3 is set at 1:2, displaying a specific discharge capacity of 129.4 mA h g^{-1} at 0.5 C and a capacity retention of 82.3% after 200 charge–discharge cycles. In addition, it still shows a high rate performance with a discharge capacity of 112.7 mA h g^{-1} at 10 C and 98.8 mA h g^{-1} at 20 C, which is attributed to an accurate Ni/Mn ratio, smaller primary particle sizes and a porous spherical morphology.

Keywords: rapid precipitation; hydrothermal treatment; mixed precipitants; spherical morphology

1. Introduction

Recently, the development of energy storage technology has played a key role in boosting the popularization of the hybrid electric vehicle (HEV) and electric vehicle (EV). As an excellent energy storage system, the lithium ion battery has increasingly aroused attention due to its high energy density, long cycle life, and environmental friendliness. However, there are still some problems, such as short capacity fading, high costs, and potential safety hazards during the course of practical application [1–5]. It has also been considered that the improvement of energy/power density of lithium ion batteries has been a significant theme, and the development of high performance cathode materials has been the main approach for resolving it [5]. As a promising cathode material for lithium ion batteries, spinel $LiNi_{0.5}Mn_{1.5}O_4$ (LNMO) has caused attracted an increasing amount of attention due to its high discharge plateau around 4.7 V, its low cost, and its high energy density (630 Wh kg^{-1}) [6,7]. Therefore, it is a competitive candidate to be applied in electric vehicles (EVs) and hybrid electric vehicles (HEVs) [8].

Various methods such as solid state [9,10], sol-gel [11–16], co-precipitation [17], and hydrothermal [18] have been increasingly reported to synthesize LNMO with different morphologies. The solid state method is the earliest and simplest way to obtain the cathode material. However, it is hard to regulate the morphology and to obtain a pure spinel phase. The sol-gel or co-precipitation method is also a common route used by researchers to prepare cathode materials with excellent electrochemical properties, which is ascribed to a feasible measure with which the materials' morphology and stoichiometry provided by the two methods can be accurately controlled. Unfortunately, the relatively tedious steps and long time also decrease their glamour [19–21]. Specially, as a simple operation, the hydrothermal method can not only regulate the morphology but also guarantee the accurate stoichiometry of LNMO cathode materials [22,23].

It is usually considered that the excellent cycling behavior of cathode materials is partially attributed to the small surface area of spherical particles, which could weaken the unexpected side reaction during the electrochemical process. Meanwhile, what leads to an excellent rate performance is the uniform electrode–electrolyte contact for Li ions fast transfer across the interface, which is more significant in spherical materials with a porous configuration [24,25]. In regulating the morphology and electrochemical performance of LNMO cathode materials, the traditional co-precipitation method is usually performed by adding the $NH_3 \cdot H_2O$ or ammonium carbonate solution drop by drop to control the spherical morphology and pH value under long-term continuous stirring [6,7,26,27], and the hydrothermal treatment is carried out by adjusting the precipitants and hydrothermal parameters. Cheng et al. synthesized LNMO cathode material with sphere-like morphology under hydrothermal conditions when Na_2CO_3 was used as a precipitant [18]. However, it showed poor electrochemical performance. Uniform LNMO microspheres were successfully prepared by Zhu et al., with NH_4HCO_3 as a precipitant using the hydrothermal method [22]. The excellent electrochemical performance fully displayed the advantage of spherical LNMO. However, the large amount of consumption and long-term dripping process of NH_4HCO_3 also needs further optimization.

Herein, a rapid precipitation method followed by a hydrothermal treatment was used to prepare the precursors of LNMO. The precursor samples were synthesized by adjusting the molar ratio of $(NH_4)_2CO_3$ to Na_2CO_3 in a mixed precipitant for evaluating the effects of ammonia from $(NH_4)_2CO_3$ as a complexing agent and Na_2CO_3 as a precipitant on the morphology and electrochemical performances of LNMO. After the hydrothermal process, the spherical morphology of $Ni_{0.25}Mn_{0.75}CO_3$ precursor was obtained. Then, through the calcination of precursors with a lithium source, the LNMO samples were synthesized.

2. Experimental

2.1. The Synthesis of $Ni_{0.25}Mn_{0.75}CO_3$ Precursors

A rapid precipitation method followed by a hydrothermal treatment is applied to synthesize the spherical $Ni_{0.25}Mn_{0.75}CO_3$ precursor. Firstly, 2.25 mmol $NiSO_4 \cdot 6H_2O$ (AR, Sinopharm Chemical Reagent Co, Shanghai, China) and 6.75 mmol $MnSO_4 \cdot H_2O$ (AR, Sinopharm Chemical Reagent Co., Shanghai, China) were ultrasonically dissolved in 25 mL of deionized water followed by the addition of 12.5 mL of ethanol to promote the dispersion of transition metal ions. Meanwhile, $(NH_4)_2CO_3$ (Aladdin, Los Angeles, CA, USA) and Na_2CO_3 (AR, Sinopharm Chemical Reagent Co., Shanghai, China) with different molar ratios (0:1, 1:2, 1:1, 2:1, and 1:0) were also ultrasonic dissolved in respectively assigned deionized water (a total of 25 mL) according to the molar ratio of mixed precipitants. The molar ratio between total carbonate and total transition metal ions was set at 1.2:1 to guarantee the complete precipitation of transition metal ions. Secondly, the $(NH_4)_2CO_3$ solution was poured into the metal salt solution followed by the same operation with an Na_2CO_3 solution to generate massive sediments. The suspension was directly transferred into 100 mL of PVDF-lined noncorrosive steel and treated at 200 °C for 12 h in the oven. Finally, we obtained the spherical $Ni_{0.25}Mn_{0.75}CO_3$ precursor after it was washed several times and dried at 60 °C overnight.

2.2. The Synthesis of LNMO Cathode Materials

The dried precursor was ground with 5% excess Li_2CO_3 (Aladdin, Los Angeles, CA, USA) for 1 h. Subsequently, the mixture was transferred to a muffle furnace and calcined at 550 °C for 3 h, 800 °C for 10 h in air (according to the TGA, as shown in Figure S1) at a heating rate of 2 °C/min. The final product, which was named after the molar ratio of $(NH_4)_2CO_3$ to Na_2CO_3 (S_{01}, S_{12}, S_{11}, S_{21}, and S_{10} corresponding to 0:1, 1:2, 1:1, 2:1, and 1:0), could be obtained after it was naturally cooled down to room temperature. The specific experimental process is diagrammatically shown in Figure 1; and more details could be found elsewhere [23,28].

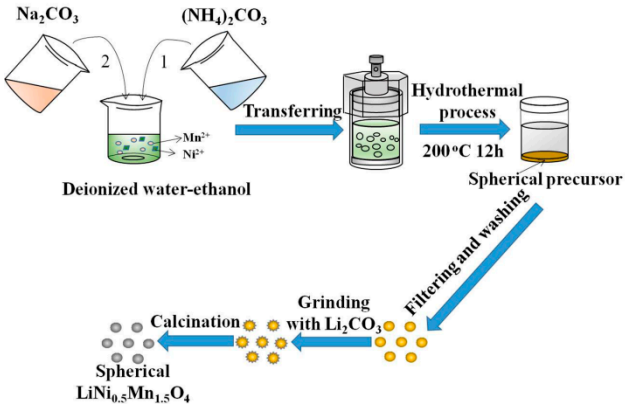

Figure 1. Diagrammatic illustration of the synthesis process for $LiNi_{0.5}Mn_{1.5}O_4$ (LNMO) cathode materials.

2.3. Materials Characterizations

The phase analysis of as-prepared LNMO cathode material was performed via X-ray powder diffraction (XRD, Microdiffractometer D8 Advance, BrukerAXS, Karlsruhe, Baden-Wurttemberg, Germany). The morphologies and particle sizes were observed with a field emission scanning electron microscope (FESEM, S-4800, Hitachi, Blackwood, NJ, USA). The components of as-prepared materials were confirmed via inductive coupled plasma atomic emission spectrometry (ICP-MS, iCAP-Qc, Thermo Fisher Scientific, Waltham, MA, USA). The Brunauer–Emmett–Teller (BET) surface areas of the materials were determined via a physisorption and chemisorption analyzer (ASAP 2020-M+C, Micromeritics Instrument Corp, Atlanta, GA, USA). The microstructure, the chemical states of Ni and Mn elements, and the thermal gravimetric of the sample with the best electrochemical performance were respectively characterized with transmission electron microscopy (TEM, Tecnai G2 F20, FEI, Hillsboro, OR, USA), X-ray photoelectron spectroscopy (XPS, K-Alpha, Thermo Fisher Scientific, Waltham, MA, USA), and thermogravimetric analysis (TGA, STA449F3, Netzsch, Selb, Bavaria, Germany), respectively. When conducting the test of TEM, the preparation of the TEM specimen was as follows: firstly, the sample of LNMO was ultrasonically dispersed with ethanol for 40 min; secondly, the sample was filtered onto a copper screen; lastly, after drying, it was tested. XPS was performed under the following conditions: chamber pressure: 8×10^{-8} Pa; take-off angle: 90°; calibration: according to the standard C 1s spectrum with a binding energy of 284.6 eV, the test value of 283.48 eV for C 1 s spectrum was calibrated. The TGA was carried out from 35 to 900 °C at a heating rate of 10 °C/min. The structural parameters and crystallite size were calculated with JADE 6.5 software, which was based on the XRD data.

2.4. Electrochemical Measurements

The electrochemical performance test was carried out by CR-2032-type coin cells including a positive electrode, a Celgard 2500 membrane, an electrolyte, and a lithium negative electrode, which were assembled in an argon-filled glove box. The positive electrode was comprised of

80% as-prepared cathode materials, 10% carbon black (Super P), and 10% polyvinylidene fluoride (PVDF), which was homogeneously mixed by a proper amount *N*-methyl-2-pyrrolidon (NMP) to form the cathode slurry. Then, the obtained slurry was coated on Al foil and vacuum-dried at 120 °C overnight. The electrolyte was 1M $LiPF_6$ dissolved in EC/DMC (1:1, volume ratio). Galvanostatic charge–discharge tests were carried out between 3.0 and 4.9 V by LAND-2010 automatic battery testers at 25 °C.

3. Results and Discussion

Figure 2 shows the XRD patterns of as-prepared LNMO materials. All the peaks can be assigned to a well-crystallized typical cubic spinel structure with a space group of Fd3m (JCPDS Card No. 80-2162). It is noteworthy that the additional minor XRD reflections at 2θ = 37.4°, 43.5°, and 63.2° can be observed on S_{01}, which is assigned to small amounts of a rock salt phase [29]. We can observe from the pattern that the integrated intensity of S_{12}, which is lower than those of S_{21} and S_{10}, higher than that of S_{11}, and similar to that of S_{01}, reveals a medium crystallinity among the five samples. Meanwhile, the structural parameters and crystallite sizes are shown in Table 1. The S_{12} exhibits a lattice parameter of 8.1723 Å and a crystallite size of 256.8 nm, corresponding to the medium crystallinity, which may result in superior electrochemical performances.

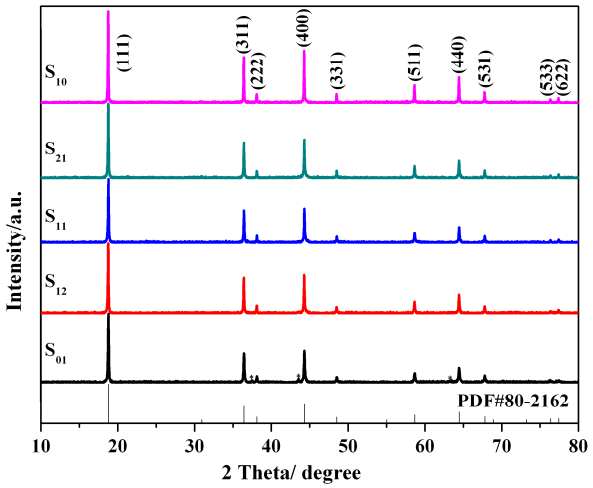

Figure 2. XRD patterns of LNMO samples prepared by mixed precipitants of $(NH_4)_2CO_3$ and Na_2CO_3 with different molar ratios.

Table 1. The structural parameters for the LNMO samples prepared by mixed precipitants of $(NH_4)_2CO_3$ and Na_2CO_3 with different molar ratios.

Samples	Lattice Parameter (Å)	Cell Volume (Å^3)	Crystallite Size (nm)
S_{01}	8.1682	544.9781	263.6
S_{12}	8.1723	545.7992	256.8
S_{11}	8.1692	545.1783	193.4
S_{21}	8.1705	545.4386	287.8
S_{10}	8.1732	545.9796	320.5

Figure 3 presents the SEM images of $Ni_{0.25}Mn_{0.75}CO_3$ precursors prepared by mixed precipitants of $(NH_4)_2CO_3$ and Na_2CO_3 with different molar ratios. We can observe that the primary particles accumulate increasingly close, and the surface of spheres is increasingly smooth from S_{01} to S_{10} at a high resolution (as shown in Figure S2). According to one of SEM images of precursors (as shown in Figure S3), we can find that there was no obvious different in the morphology among the precursors before and after hydrothermal treatment. Additionally, what the images clearly display at

low resolution is that the morphologies of the spheres become increasingly complete and uniform-sized. When the molar ratio of $(NH_4)_2CO_3$ to Na_2CO_3 was set at 0:1, it can be clearly observed that the precursor shows a high degree of fragmentation. The precursor of S_{12} and the other three precursors all show complete spherical morphologies with a trend of increasingly uniform primary particles. This interesting phenomenon might be attributed to the complexation of ammonia for $(NH_4)_2CO_3$ with nickel ions during the hydrothermal process, which can contribute to the uniform precipitation with spherical morphology. The complexation of ammonia with Ni and Mn also slow down the precipitation process and simultaneously favor the dissolution process during hydrothermal treatment when the content of ammonia increases, and therefore increase the compactness of the primary particles, which can influence the morphology and particle size during the calcination process. However, the increased concentration of ammonia will seriously hinder the completed deposition of nickel ions, and lead to a deficiency of nickel [7]. To further confirm the deficiency of nickel, ICP-MS measurement was carried out, and the detailed results regarding the content of nickel and manganese are presented in Table 2, which shows that the Ni/Mn ratio presents a decreasing trend from S_{01} to S_{10}. The S_{12} delivered an Ni/Mn ratio of 1.01:3, which is closest to the theoretical value, while the ratio of 0.9:3 for 1:0 reveals that about 10% of nickel ions were lost in the solution.

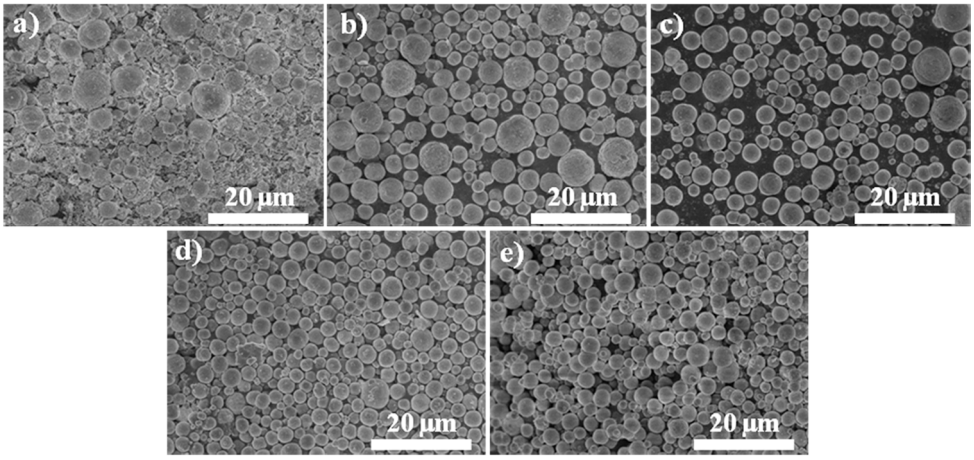

Figure 3. Low-resolution SEM images of spherical precursor prepared by mixed precipitants of $(NH_4)_2CO_3$ and Na_2CO_3 with different molar ratios: (**a**) 0:1; (**b**) 1:2; (**c**) 1:1; (**d**) 2:1; (**e**) 1:0.

Table 2. ICP-MS results of the LNMO samples prepared by mixed precipitants of $(NH_4)_2CO_3$ and Na_2CO_3 with different molar ratios.

Samples	Ni/Mn (Atomic Ratio)	Ni/Mn (fix Mn = 3)
S_{01}	0.5098:1.4902	1.03:3
S_{12}	0.5046:1.4954	1.01:3
S_{11}	0.4921:1.5079	0.98:3
S_{21}	0.4812:1.5189	0.95:3
S_{10}	0.4616:1.5385	0.90:3

Figure 4 indicates the SEM images of as-prepared LNMO materials. The low-resolution images indicate that the spherical morphologies of as-prepared samples are basically well maintained and showed a trend that is consistent with the precursors. What we can further observe from the high-resolution images is that the primary sizes of S_{12} are obviously larger than those of S_{11} while smaller than those of S_{21} and S_{10}. In addition, the samples of S_{01} and S_{12} show the loose accumulation between primary particles with small pores distributed on the surfaces of microspheres, which may contribute to the improvement of rate performances. Nevertheless, the opposite status, the compact accumulation between particles without pores observed on the surfaces of the

microspheres, is displayed by the other samples. This observation result agrees with the data of the BET surface areas, which is enumerated in Table 3. It can be evidently observed from Table 3 that a decreasing trend from S_{01} (4.3612 m^2 g^{-1}) to S_{10} (2.8820 m^2 g^{-1}) is regularly presented.

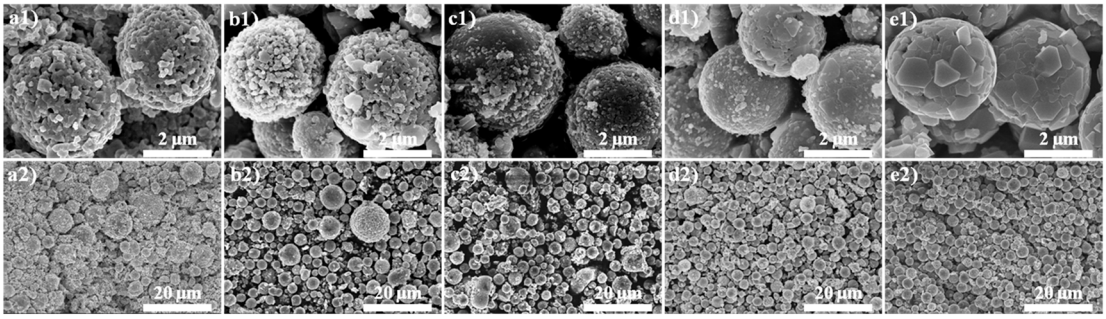

Figure 4. High- and low-resolution SEM images of (**a1**,**a2**) S_{01}; (**b1**,**b2**) S_{12}; (**c1**,**c2**) S_{11}; (**d1**,**d2**) S_{21}; (**e1**,**e2**) S_{10}.

Table 3. BET surface areas of the LNMO samples prepared by mixed precipitants of $(NH_4)_2CO_3$ and Na_2CO_3 with different molar ratios.

Samples	S_{01}	S_{12}	S_{11}	S_{21}	S_{10}
BET/m^2 g^{-1}	4.3612	3.5522	3.1217	3.0837	2.8820

To further analyze the microstructure and surface chemical states of S_{12}, TEM (Figure 5a), HRTEM (Figure 5b), and XPS (Figure 6) were carried out. Figure 5a presents a typical spherical structure, which corresponds to the SEM image (Figure 4b1). The high-resolution TEM image (Figure 5b) shows obvious lattice fringes (0.47 nm), which matches the (111) plane of spinel LNMO.

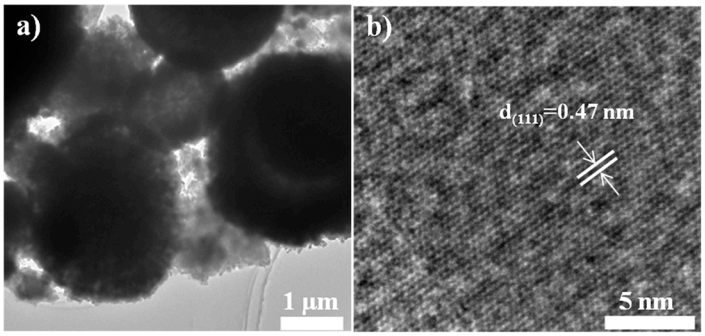

Figure 5. TEM (**a**) and high-resolution TEM (**b**) of S_{12}.

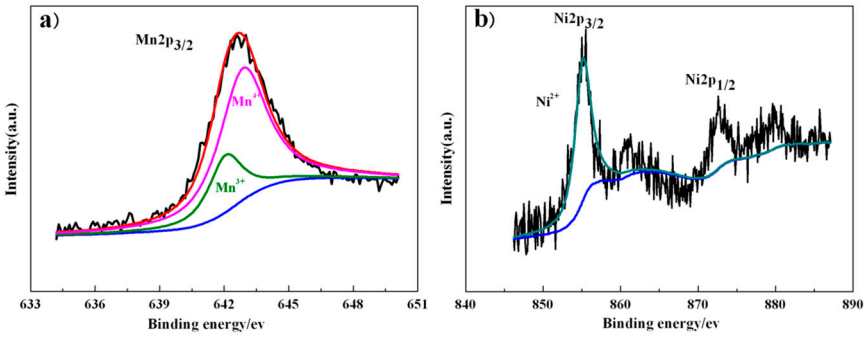

Figure 6. X-ray photoelectron spectra of (**a**) Mn 2p and (**b**) Ni 2p of S_{12}.

Figure 6a shows the XPS spectra of Mn 2p, revealing that the binding energies of 642.1 eV and 642.9 eV, which respectively correspond to Mn^{3+} and Mn^{4+}, are assigned to the major peak of Mn $2p_{3/2}$, near 641.9 eV for Mn^{3+} and 642.9 eV for Mn^{4+}, which have been reported previously [21]. The coexistence of Mn^{4+} and Mn^{3+} observed from the XPS spectra of Mn 2p is well consistent with the discharge capacity curve in Figure 7a. As Figure 6b shows, the major peak assigned to Ni $2p_{3/2}$ binding energy is located at 855.1 eV, whose value is close to those reported for LNMO (854.8 eV) [30].

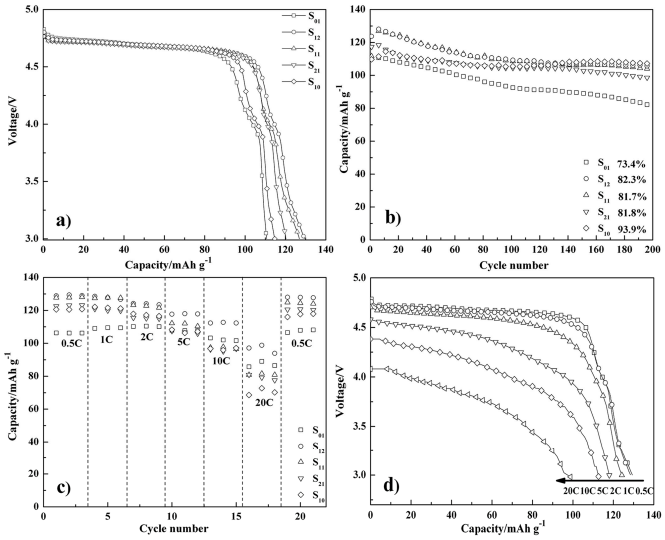

Figure 7. (**a**) The galvanostatic discharge curves (highest discharge capacity) of the LNMO samples prepared by mixed precipitants of $(NH_4)_2CO_3$ and Na_2CO_3 with different molar ratios; (**b**) the cycle performances of the LNMO samples at 0.5 C; (**c**) the rate performances of the LNMO samples at various C-rates; (**d**) the discharge curves of S_{12} at different C-rates.

As shown in Figure 7, different electrochemical performances of as-prepared LNMO cathode materials were measured by galvanostatic charge–discharge. According to Figure 7a, the as-prepared cathode materials all exhibit a typical discharge capacity curve of Fd3m-type spinel LNMO with a dominate discharge plateau around 4.7 V attributed to Ni^{2+}/Ni^{4+} redox couple and a weak plateau around 4 V corresponds to the Mn^{3+}/Mn^{4+} redox couple [31]. It is worth noticing that some samples show a sloping area below ~3.5 V, which could be an indication of the existence of a layered phase [32]. The highest specific discharge capacity of five samples are 110.7, 129.4, 126.9, 120.3, and 114.7 mAh g^{-1} with a charge/discharge at 0.5 C, which displays the superiority of S_{12} in comparison to the other samples. It may be due to the awful spherical morphology that S_{01} shows the lowest discharge capacity, while the discharge capacity of S_{11}, S_{21}, and S_{10} present a decreasing trend, which could be ascribed to the deficiency of nickel.

We can observe from Figure 7b that the discharge capacity retention of five samples respectively remain 73.4%, 82.3%, 81.7%, 81.8%, and 93.9% after 200 charge–discharge cycles at 0.5 C. S_{12} shows favorable cycling stability and S_{10} exhibits the best result, while S_{01} shows the worst cycling stability among all five LNMO cathode materials, which may also be ascribed to the broken spherical morphology. The LNMO cathode material with a relatively complete spherical morphology and higher crystallinity can exhibit better cycling stability, which could be attributed to the smaller contact area of the electrode–electrolyte. The small specific surface area will contribute to weakening the unexpected side reaction during the electrochemical process and mitigate the dissolution of transition metal ions [33]. Moreover, an increasing discharge capacity around the first 10 cycles can be observed from samples except S_{01}, which indicates that a longer wetting and electrochemical activation process is necessary for micron-sized spherical particles [34].

The rate performances of LNMO cathode materials from 0.5 to 20 C (the charge rate is fixed at 0.5 C) are shown in Figure 7c. Under high current density, the discharge capacities of S_{12} still are 112.7 mAh g^{-1} at 10 C and 98.8 mAh g^{-1} at 20 C, which displays the best rate performance in comparison to other samples. It indicates that LNMO cathode materials with a porous spherical morphology and smaller primary particle sizes could contribute to the infiltration of the electrolyte and the increase in the contact area between the electrode and electrolyte [35], which provides a relatively short transport length for Li ions. The results of all electrochemical performance tests fully demonstrate that S_{12} is the most appropriate molar ratio of $(NH_4)_2CO_3$ to Na_2CO_3 for synthesizing LNMO cathode material, corresponding to the highest discharge capacity, favorable cycling stability, and the best rate performance.

4. Conclusions

In general, the LNMO with spherical morphology has been successfully synthesized by a rapid precipitation and hydrothermal method with $(NH_4)_2CO_3$ and Na_2CO_3 as mixed precipitants followed by a high-temperature calcination with a lithium source. The spherical morphology and crystallinity of the as-prepared samples can be greatly influenced by the molar ratio of $(NH_4)_2CO_3$ to Na_2CO_3. The LNMO cathode material prepared with 1:2 for $(NH_4)_2CO_3$ to Na_2CO_3 displayed an accurate Ni/Mn ratio, smaller primary particle sizes, and a porous spherical morphology, and delivered the highest discharge capacity, favorable cycling stability, and the best rate performance, corresponding to 129.4 mAh g^{-1} at 0.5 C, with a capacity retention of 82.3% after 200 charge–discharge cycles, 112.7 mAh g^{-1} at 10 C, and 98.8 mAh g^{-1} at 20 C, respectively. Thus, a simple and effective route for the controllable preparation of spherical high-voltage LNMO cathode materials was successfully developed.

Supplementary Materials: The following are available online at www.mdpi.com/2073-4352/7/9/275/s1. Figure S1: TG curve of heating the mixture of precursor and lithium source for mixed precipitants of $(NH_4)_2CO_3$ and Na_2CO_3 with molar ratio of 1:2, Figure S2: High resolution SEM images of spherical precursors prepared by mixed precipitants of $(NH_4)_2CO_3$ and Na_2CO_3 with different molar ratios: (**a**) 0:1; (**b**) 1:2; (**c**) 1:1; (**d**) 2:1; (**e**) 1:0. Figure S3: High resolution SEM images of spherical precursors before (**a**) and after (**b**) hydrothermal treatment prepared by mixed precipitants of $(NH_4)_2CO_3$ and Na_2CO_3 with molar ratio of 2:1.

Acknowledgments: The authors appreciate the financial support of the "100 Talents" program of Chinese Academy of Sciences and "YZ201641".

Author Contributions: Wenchao Yan and Yongcheng Jin conceived and designed the experiments; Yang Shu performed the experiments; Yang Shu and Jicheng Jiang analyzed the data; Haisong Wang, Deye Sun, and XiaoDi Ma contributed reagents/materials/analysis tools; Yang Shu wrote the paper.

Conflicts of Interest: The authors declare no conflict of interest.

References

1. Luo, Y.; Lu, T.L.; Zhang, Y.X.; Yan, L.Q.; Mao, S.S.; Xie, J.Y. Surface-segregated, high-voltage spinel lithium-ion battery cathode material $LiNi_{0.5}Mn_{1.5}O_4$ cathodes by aluminium doping with improved high-rate cyclability. *J. Alloys Compd.* **2017**, *703*, 289–297. [CrossRef]
2. Sun, P.; Ma, Y.; Zhai, T.Y.; Li, H.Q. High performance $LiNi_{0.5}Mn_{1.5}O_4$ cathode by Al-coating and Al^{3+}-doping through a physical vapor deposition method. *Electrochim. Acta* **2016**, *191*, 237–246. [CrossRef]
3. Alva, G.; Kim, C.J.; Yi, T.H.; Cook, J.B.; Xu, L.P.; Nolis, G.M.; Cabana, J. Surface Chemistry Consequences of Mg-Based Coatings on $LiNi_{0.5}Mn_{1.5}O_4$ Electrode Materials upon Operation at High Voltage. *J. Phys. Chem. C* **2014**, *118*, 10596–10605. [CrossRef]
4. Tao, S.; Kong, F.J.; Wu, C.Q.; Su, X.Z.; Xiang, T.; Chen, S.M.; Hou, H.H.; Zhang, L.; Fang, Y.; Wang, Z.C.; et al. Nanoscale TiO_2 membrane coating spinel $LiNi_{0.5}Mn_{1.5}O_4$ cathode material for advanced lithium-ion batteries. *J. Alloys Compd.* **2017**, *705*, 413–419. [CrossRef]
5. Ma, J.; Hu, P.; Cui, G.L.; Chen, L.Q. Surface and Interface Issues in Spinel $LiNi_{0.5}Mn_{1.5}O_4$: Insights into a Potential Cathode Material for High Energy Density Lithium Ion Batteries. *Chem. Mater.* **2016**, *28*, 3578–3606. [CrossRef]

6. Sun, Y.Y.; Yang, Y.F.; Zhao, X.C.; Shao, H.X. Synthesis and electrochemical characterization of $LiNi_{0.5}Mn_{1.5}O_4$ by one-step precipitation method with ammonium carbonate as precipitating agent. *Electrochim. Acta* **2011**, *56*, 5934–5939. [CrossRef]
7. Zhu, Z.; Zhang, D.; Yu, H.Y. Preparation of spherical hierarchical $LiNi_{0.5}Mn_{1.5}O_4$ with high electrochemical performances by a novel composite co-precipitation method for 5V lithium ion secondary batteries. *Electrochim. Acta* **2014**, *115*, 290–296. [CrossRef]
8. Liu, Y.Z.; Zhang, M.H.; Xia, Y.G.; Qiu, B.; Liu, Z.P.; Li, X. One-step hydrothermal method synthesis of core–shell $LiNi_{0.5}Mn_{1.5}O_4$ spinel cathodes for Li-ion batteries. *J. Power Sources* **2014**, *256*, 66–71. [CrossRef]
9. Fang, H.S.; Wang, Z.X.; Li, X.H.; Guo, H.J.; Peng, W.J. Low temperature synthesis of $LiNi_{0.5}Mn_{1.5}O_4$ spinel. *Mater. Lett.* **2006**, *60*, 1273–1275. [CrossRef]
10. Agostini, M.; Matic, A.; Panero, S.; Croce, F.; Gunnella, R.; Reale, P.; Brutti, S. A mixed mechanochemical-ceramic solid-state synthesis as simple and cost effective route to high-performance $LiNi_{0.5}Mn_{1.5}O_4$ spinels. *Electrochim. Acta* **2017**, *235*, 262–269. [CrossRef]
11. Sun, Y.Y.; Yang, Y.F.; Zhan, H.; Shao, H.X.; Zhou, Y.H. Synthesis of high power type $LiMn_{1.5}Ni_{0.5}O_4$ by optimizing its preparation conditions. *J. Power Sources* **2010**, *195*, 4322–4326. [CrossRef]
12. Pang, Q.; Fu, Q.; Wang, Y.H.; Zhang, Y.Q.; Zou, B.; Du, F.; Chen, G.; Wei, Y.J. Improved Electrochemical Properties of Spinel $LiNi_{0.5}Mn_{1.5}O_4$ Cathode Materials by Surface Modification with RuO_2 Nanoparticles. *Electrochim. Acta* **2015**, *152*, 240–248. [CrossRef]
13. Kiziltas-Yavuz, N.; Bhaskar, A.; Dixon, D.; Yavuz, M.; Nikolowski, K.; Lu, L.; Eichel, R.-A.; Ehrenberg, H. Improving the rate capability of high voltage lithium-ion battery cathode material $LiNi_{0.5}Mn_{1.5}O_4$ by ruthenium doping. *J. Power Sources* **2014**, *267*, 533–541. [CrossRef]
14. Zhong, G.B.; Wang, Y.Y.; Zhang, Z.C.; Chen, C.H. Effects of Al substitution for Ni and Mn on the electrochemical properties of $LiNi_{0.5}Mn_{1.5}O_4$. *Electrochim. Acta* **2011**, *56*, 6554–6561. [CrossRef]
15. Zhong, G.B.; Wang, Y.Y.; Zhao, X.J.; Wang, Q.S.; Yu, Y.; Chen, C.H. Structural, electrochemical and thermal stability investigations on $LiNi_{0.5-x}Al_{2x}Mn_{1.5-x}O_4$ ($0 \leq 2x \leq 1.0$) as 5 V cathode materials. *J. Power Sources* **2012**, *216*, 368–375. [CrossRef]
16. Choi, H.W.; Kim, S.J.; Rim, Y.H.; Yang, Y.S. Effect of Lithium Deficiency on Lithium-Ion Battery Cathode $Li_xNi_{0.5}Mn_{1.5}O_4$. *J. Phys. Chem. C* **2015**, *119*, 27192–27199. [CrossRef]
17. Gao, J.; Li, J.J.; Song, F.; Lin, J.X.; He, X.M.; Jiang, C.Y. Strategy for synthesizing spherical $LiNi_{0.5}Mn_{1.5}O_4$ cathode material for lithium ion batteries. *Mater. Chem. Phys.* **2015**, *152*, 177–182. [CrossRef]
18. Cheng, J.L.; Li, X.H.; Wang, Z.X.; Guo, H.J. Hydrothermal synthesis of $LiNi_{0.5}Mn_{1.5}O_4$ sphere and its performance as high-voltage cathode material for lithium ion batteries. *Ceram. Int.* **2016**, *42*, 3715–3719. [CrossRef]
19. Hoshina, K.; Yoshima, K.; Kotobuki, M.; Kanamura, K. Fabrication of $LiNi_{0.5}Mn_{1.5}O_4$ thin film cathode by PVP sol–gel process and its application of all-solid-state lithium ion batteries using $Li_{1+x}Al_xTi_{2-x}(PO_4)_3$ solid electrolyte. *Solid State Ion.* **2012**, 209–210, 30–35. [CrossRef]
20. Fang, J.C.; Xu, Y.F.; Xu, G.L.; Shen, S.Y.; Li, J.T.; Huang, L.; Sun, S.G. Fabrication of densely packed $LiNi_{0.5}Mn_{1.5}O_4$ cathode material with excellent long-term cycleability for high-voltage lithium ion batteries. *J. Power Sources* **2016**, *304*, 15–23. [CrossRef]
21. Yao, Y.L.; Liu, H.C.; Li, G.C.; Peng, H.R.; Chen, K.Z. Multi-shelled porous $LiNi_{0.5}Mn_{1.5}O_4$ microspheres as a 5 V cathode material for lithium-ion batteries. *Mater. Chem. Phys.* **2014**, *143*, 867–872. [CrossRef]
22. Zhu, X.B.; Li, X.N.; Zhu, Y.C.; Jin, S.S.; Wang, Y.; Qian, Y.T. Porous $LiNi_{0.5}Mn_{1.5}O_4$ microspheres with different pore conditions: Preparation and application as cathode materials for lithium-ion batteries. *J. Power Sources* **2014**, *261*, 93–100. [CrossRef]
23. Zhao, E.Q.; Liu, W.; Guo, Y.D.; Xu, Y.J.; Yan, W.C.; Sun, D.Y.; Jin, Y.C. Rapid hydrothermal and post-calcination synthesis of well-shaped $LiNi_{0.5}Mn_{1.5}O_4$ cathode materials for lithium ion batteries. *J. Alloys Compd.* **2017**, *695*, 3393–3401. [CrossRef]
24. Qian, Y.X.; Deng, Y.F.; Shi, Z.C.; Zhou, Y.B.; Zhuang, Q.C.; Chen, G.H. Sub-micrometer-sized $LiMn_{1.5}Ni_{0.5}O_4$ spheres as high rate cathode materials for long-life lithium ion batteries. *Electrochem. Commun.* **2013**, *27*, 92–95. [CrossRef]
25. Nageswaran, S.; Keppeler, M.; Kim, S.J.; Srinivasan, M. Morphology controlled Si-modified $LiNi_{0.5}Mn_{1.5}O_4$ microspheres as high performance high voltage cathode materials in lithium ion batteries. *J. Power Sources* **2017**, *346*, 89–96. [CrossRef]

26. Luo, W.B. Effect of morphology on the physical and electrochemical properties of the high-voltage spinel cathode $LiMn_{1.5}Ni_{0.5}O_4$. *J. Alloys Compd.* **2015**, *636*, 24–28. [CrossRef]
27. Zhang, M.H.; Wang, J.; Xia, Y.G.; Liu, Z.P. Microwave synthesis of spherical spinel $LiNi_{0.5}Mn_{1.5}O_4$ as cathode material for lithium-ion batteries. *J. Alloys Compd.* **2012**, *518*, 68–73. [CrossRef]
28. Yan, W.C.; Jiang, J.C.; Liu, W.; Sun, D.Y.; Zhao, E.Q.; Jin, Y.C.; Kanamura, K. Effect of precipitators on the morphologies and electrochemical properties of $Li_{1.2}Mn_{0.54}Ni_{0.13}Co_{0.13}O_2$ via rapid nucleation and post-solvothermal method. *Electrochim. Acta* **2017**, *224*, 161–170. [CrossRef]
29. Keppeler, M.; Nageswaran, S.; Kim, S.J.; Srinivasan, M. Silicon Doping of High Voltage Spinel $LiNi_{0.5}Mn_{1.5}O_4$ towards Superior Electrochemical Performance of Lithium Ion Batteries. *Electrochim. Acta* **2016**, *213*, 904–910. [CrossRef]
30. Liu, G.Q.; Du, Y.L.; Liu, W.B.; Wen, L. Study on the action mechanism of doping transitional elements in spinel $LiNi_{0.5}Mn_{1.5}O_4$. *Electrochim. Acta* **2016**, *209*, 308–314. [CrossRef]
31. Deng, J.C.; Xu, Y.L.; Xiong, L.L.; Li, L.; Sun, X.F.; Zhang, Y. Improving the fast discharge performance of high-voltage $LiNi_{0.5}Mn_{1.5}O_4$ spinel by Cu^{2+}, Al^{3+}, Ti^{4+} tri-doping. *J. Alloys Compd.* **2016**, *677*, 18–26. [CrossRef]
32. Chemelewski, K.R.; Lee, E.S.; Li, W.; Manthiram, A. Factors Influencing the Electrochemical Properties of High-Voltage Spinel Cathodes: Relative Impact of Morphology and Cation Ordering. *Chem. Mater.* **2013**, *25*, 2890–2897. [CrossRef]
33. Yan, W.C.; Jiang, J.C.; Liu, W.; Yan, X.; Sun, D.Y.; Jin, Y.C.; Wang, J.; Xiang, L.; Munakata, H.; Kanamura, K. Synthesis and Evaluation of Microspherical $Li_{1.2}Mn_{0.54}Co_{0.13}Ni_{0.13}O_2$ through Carbon Dioxides-assisted Co-precipitation Method for Lithium-ion Battery. *Electrochim. Acta* **2016**, *212*, 16–24. [CrossRef]
34. Liu, H.D.; Wang, J.; Zhang, X.F.; Zhou, D.; Qi, X.; Qiu, B.; Fang, J.H.; Kloepsch, R.; Schumacher, G.; Liu, Z.P.; et al. Morphological Evolution of High-Voltage Spinel $LiNi_{0.5}Mn_{1.5}O_4$ Cathode Materials for Lithium-Ion Batteries: The Critical Effects of Surface Orientations and Particle Size. *ACS Appl. Mater. Interfaces* **2016**, *8*, 4661–4675. [CrossRef] [PubMed]
35. Xu, Y.H.; Zhao, S.X.; Deng, Y.F.; Deng, H.; Nan, C.W. Improved electrochemical performance of 5 V spinel $LiNi_{0.5}Mn_{1.5}O_4$ microspheres by F-doping and Li_4SiO_4 coating. *J. Materiomics* **2016**, *2*, 265–272. [CrossRef]